INTERNATIONAL JOURNAL OF PRECISION ENGINEERING AND MANUFACTURING Vol. 18, No. 7, pp. 979-986 JULY 2017 / 979

REGULAR PAPER

DOI: 10.1007/s12541-017-0115-3
ISSN 2234-7593 (Print) / 2005-4602 (Online)

Modeling and Numerical Simulation of Afterburning of Thermobaric Explosives in a Closed Chamber

Chang-Kee Kim[1], Ming-Chia Lai[2], Zeng-Chan Zhang[3], Grant Cook, Jr.[3], and Kyoung-Su Im[3,#]

1 Warhead & Fuze Technology Directorate, Agency for Defense Development, Yuseong P.O. Box 35-5, Daejeon, 34188, South Korea
2 Department of Mechanical Engineering, Wayne State University, Detroit, MI, 48202, USA
3 Livermore Software Technology Corp., Livermore, CA 94551, USA
Corresponding Author / E-mail: ksim@lstc.com, TEL: +1-925-456-2445

KEYWORDS: TBX, Afterburning, Modeling, Heterogeneous, Blast

An Eulerian-Lagrangian simulation of the thermobaric explosion and the propagating detonation waves with aluminum particle combustion in a closed chamber is carried out and validated very favorably with the pressure histories measured experimentally. A novel numerical framework based on the space-time conservation-element and solution-element method (CE/SE) was employed to simulate the complex detonating flow with detailed chemistry. A discrete particle technique was adopted with either a mono-dispersed or poly-dispersed particle distribution. The results between the experiment and simulation on pressure histories and corresponding impulse forces are compared and showed good agreement. In addition, the effects of metal combustion on afterburning were discussed in detail in terms of the reaction mechanisms and particle dynamics.

Manuscript received: March 10, 2016 / Revised: March 7, 2017 / Accepted: March 10, 2017

NOMENCLATURE

C_D = drag coefficient
c_p = specific heat coefficient
D = drag function or diameter
d_0 = particle diameter
e = specific internal energy
E_t = specific total energy
f_m^x, f_m^y, f_m^z = primitive flux vectors
h = specific enthalpy
K = burning rate constant
m_p = particle mass
q_l = net rate of progress
r = particle radius
R_e = Reynolds number
$S(u_m)$ = particle source term vector
$W(u_m)$ = chemical source term vector
W_k = molar weight
u, v, w = flow velocities
x, y, z = spatial coordinates
y_k = mass fraction
ρ = density
Ω_k = production rate
ϕ = volume fraction

Subscripts **Superscripts**

g = gas
x, y, z = spatial direction
k = species index
l = liquid
o = initial value
p = particle index

1. Introduction

Heterogeneous combustion (i.e., solid and gas or liquid and gas) has a wide range of applications such as solid rocket propulsion, combustion instability control, underwater explosion, and high energy explosion.[1-6] Among several possible combinations, the thermobaric explosive (TBX)

composed of trinitrotoluene (TNT) and energetic metal particles (typically aluminum) is a widely used explosive and is of great importance in the safety, mining, and defense industries. After the onset of the detonation developed from the initial burst charge, TBX is typically accompanied by a secondary combustion, or afterburning, which releases more energy than the initial bursting charge explosion. As a result, a fairly large combustion area within the fireball radius is sustained until all combustion products are consumed.[7] The flow physics involved in an afterburning of TBX is very complicated, including the transient processes of blast wave propagation and reflection, metal combustion, multiphase turbulent mixing, and multimode chemical reaction. However, due to a dearth of the proper experimental tools caused by the methodological difficulty of acquiring quantitative data during the explosion, there are only very few available studies. Moreover, the difficulties in detailed understanding of the afterburning process of TBX arise from the lack of 1) appropriate heterogeneous multiphase combustion models with realistic particle dynamics, and 2) proper solid metal combustion models such as a burning rate law of metal particles.

To simulate heterogeneous multiphase combustion in the afterburning of TBX, the metal particles interacting with detonating gas can be most realistically modeled in a Lagrangian reference frame in which the effects of pressure and the speed of sound on individual particle can be neglected.[8] Simultaneously, the continuity, momentum, and energy equations must be solved for all metal particles, and their burning rates and locations accurately traced. As a result, huge computational capacity is required. As an alternative to resolve the issue, the particle phase is often treated as a continuous phase in which the particles are modeled as a fluid in a Eulerian frame to minimize the computational cost. Such an investigation with the dispersal of inert solid particles in blast propagation was reported by Zhang et al..[9] However, in their approach, a heuristic equation of state (EOS) was required which is neither based on theoretical analysis nor validated by experimental data. Furthermore, since the particles are represented by a single average size for each computational cell, the critical particle dynamics related to the afterburning performance in TBX is over-simplified.

Another approach to resolve the problem is to use a discrete particle or computational particle model, which has a finite number of particles having the same physical characteristics such as diameter, velocity, and temperature and thus, the total number of sampling particles represent all physical particles in the domain.[10] Moreover, increased computational power in the future will enable to simulate even more discrete particle samples with fewer discrete child particles.

Proper modeling of aluminum combustion and the burning rate law has been an ongoing subject since Brzustowski and Glassman[11] developed the first model in the 1960s. A simplified theoretical model considering surface condensation depending on the direction of the bulk gaseous velocities was developed by Law.[12] Since the afterburning of TBX consists of multi-physics interactions between the blast waves and the dispersed particles, simultaneously including shock physics, a simplified particle model with an implicit burning mechanism such as Glassman's hypothesis[13] could be a more realistic choice than a complicated model with detailed kinetic reaction mechanisms developed for a single aluminum particle. For example, an aluminum particle model akin to Law's formulation was implemented into the second-order hydrodynamic automatic mesh refinement code by Needham et al..[14] In their case, the particle-burning rate was fit to a third-order polynomial as a function of the oxidizer concentration in surrounding particles supported by experimental data. Another simplified burning model for the aluminum particle that is suitable in both the quiescent and high-speed gas flow was proposed based on the reduced-film approximation. Calibrated with experimental data, Khasainov and Veyssiere[15] employed this model in gaseous explosive mixtures with aluminum particles in suspension. Recently, Zhang, et al.[16] developed a hybrid reaction model by combining Khasainov's diffusion rate with the surface kinetic rate in Arrhenius form, and successfully demonstrated it in modeling both detonation initiation and the deflagration-to-detonation transition.

In the present study, we developed the model and simulation of afterburning processes of TBX based on realistic particle dynamics and a solid metal combustion model, which are suitable for high-speed detonating flow. A new numerical framework based on the space-time conservation-element and solution-element (CE/SE) method[17] was employed to simulate the complex detonating blast waves with multi-species chemically reacting flow in a Eulerian reference frame. A discrete particle technique calibrated with total metal mass in a Lagrangian reference frame was employed in conjunction with either a mono-dispersed or poly-dispersed particle size distribution sampled by a probability density function (PDF) to demonstrate the size distribution effects. Moreover, the current developed model was validated with experimental data in a closed chamber test. With the confidence of the validation, the effects of thermodynamics and particle dynamics parameters on afterburning performance were investigated and discussed.

2. Model Equations

2.1 Gas phase

In the situation where the dispersed phase has a relatively small or negligible volume fraction, with approximately spherical particles so that the collision and any breakup effects can be neglected, the macroscopic mass density (i.e., $\rho = \alpha_g \rho_g$, $\alpha_g \approx 1$) is valid for the gas mixture. Thus, we employed the 3-D unsteady, multi-species reactive Euler equations as the gas phase model governing the detonating blast propagation with energetic metal particle combustion.[18]

$$\frac{\partial u_m}{\partial t}+\frac{\partial f_m^x}{\partial x}+\frac{\partial f_m^y}{\partial y}+\frac{\partial f_m^z}{\partial z}=S(u_m)+W(u_m) \quad m=1,2,3,\ldots,n_{s-1}+5 \tag{1}$$

where t, x, y and z are time, x-, y-, and z-direction coordinates, respectively. u_m, f_m^x, f_m^y, and f_m^z, m = 1, 2, 3, …, $n_{s\text{-}1}$+5 are the primitive variable- and flux-vector corresponding to x-, y-, and z-directions given by,

$$\begin{aligned} u_m &= [\rho, \rho u, \rho v, \rho w, E_t, \rho y_1, \ldots, \rho y_{n_{s-1}}]^T \\ f_m^x &= [\rho u, \rho u^2+p, \rho uv, \rho uw, (E_t+p)u, \rho u y_1, \ldots, \rho u y_{n_{s-1}}]^T \\ f_m^y &= [\rho v, \rho vu, \rho v^2+p, \rho vw, (E_t+p)v, \rho v y_1, \ldots, \rho v y_{n_{s-1}}]^T \\ f_m^z &= [\rho w, \rho wu, \rho wv, \rho w^2+p, (E_t+p)w, \rho w y_1, \ldots, \rho w y_{n_{s-1}}]^T \end{aligned} \tag{2}$$

where, ρ, u, v, w, p, and E_t are the density, x-, y-, and z-velocity

components, pressure, and the total energy per unit volume of the gas mixture, respectively. $y_k = \rho_k / \rho$, $k = 1, 2, \ldots, n_s$ (where ρ_k is the mass concentration of species k, and n_s is the number of species) is the mass fraction of species k. The total energy E_t can be expressed as

$$E_t = \rho\left(e + \frac{1}{2}u_i u_i\right) \quad i = x, y, z \tag{3}$$

where $e = \Sigma_{k=1}^{n_s} y_k e_k$ is the specific internal energy of the mixture and e_k is the specific internal energy of species k. From the thermodynamics relation, the specific internal energy for the mixture can be expressed as

$$e = h - \frac{p}{\rho} = \sum_{k=1}^{n_s} y_k h_k - \frac{p}{\rho} \tag{4}$$

where h is the specific enthalpy of the mixture, and $h_k = \int_{T_{ref}}^{T} c_{pk} dT + h_{fk}$ is the specific enthalpy of species k. c_{pk}, $k = 1, 2, \ldots, n_s$ that appear in the specific enthalpy definition are the specific heat coefficients at constant pressure.[19] By using Eq. (4), it is not necessary to add the heat of combustion as a source term in the energy equation, Eq. (1). However, the combustion temperature T (which has to be calculated from an implicit equation utilizing Newton's method) must be determined prior to the pressure calculation.

The term, $S(u_m)$ is the coupling source term vector due to solid metal particles, and $W(u_m)$ is the chemical source term vector described as,

$$\begin{aligned} S(u_m) &= [s_1, s_2, s_3, s_4, s_5, \ldots, s_k, \ldots]^T \\ W(u_m) &= [0, 0, 0, 0, 0, \rho\Omega_1, \ldots, \rho\Omega_{n_s-1}]^T \end{aligned} \tag{5}$$

where s_1, s_2, s_3, s_4, s_5, and s_k ($k = Al$) are the exchange terms representing the mass, x-, y-, and z-momentum, total energy, and the k-th species corresponding to aluminum vaporization. By taking volume averages over all particles in a control volume, the source term components can be expressed with a labeling subscript p.[18]

$$\begin{aligned} s_1 &= -\frac{1}{V}\sum_p \dot{m}_p \\ s_i &= -\frac{1}{V}\sum_p \frac{d(m_p u_{p,i})}{dt} \quad i = x, y, z \\ s_5 &= -\frac{1}{V}\sum_p \frac{d(m_p E_p)}{dt} \\ s_k &= s_1 \end{aligned} \tag{6}$$

where V is the volume of a computational cell, m_p (= $4/3\pi\rho_p r_p^3$, where ρ_p is the particle density, and r_p is the particle radius) the particle mass, $u_{p,i}$, $i = x$, y, z the particle velocity components for the x-, y-, and z-directions, respectively.

The components, Ω_k, is the production rate of species k, which is given by some kinetic rate law.

$$\Omega_k = \frac{W_k \dot{\omega}_k}{\rho} \tag{7}$$

where W_k is the molar mass of species k and $\dot{\omega}_k$ is the net molar production rate of species k. For a system of reacting ideal gas, calculation of $\dot{\omega}_k$ requires a detailed mechanism of elementary reactions, having the general form,

$$\sum_{k=1}^{n_s} \nu'_{kl} X_k \rightleftharpoons \sum_{k=1}^{n_s} \nu''_{kl} X_k, \quad l = 1, \ldots, n_r \tag{8}$$

where ν'_{kl} and ν''_{kl} are the forward and backward stoichiometric coefficients respectively, X_k is the chemical symbol for species k, and n_r is the total number of reactions in the mechanism. Then the net molar production rate of species k is given by,

$$\dot{\omega}_k = \sum_{l=1}^{n_r} \nu_{kl} q_l \quad k = 1, \ldots, n_s \tag{9a}$$

with, $q_l = k_{fl}\prod_{k=1}^{n_s}[X_k]^{\nu'_{kl}} - k_{bl}\prod_{k=1}^{n_s}[X_k]^{\nu''_{kl}}$ (9b)

where ν_{ki} (= $\nu''_{kl} - \nu'_{kl}$), and q_l is the net rate of progress for reaction l. k_{fl} and k_{bl} are the forward and backward rate coefficient of reaction l, and $[X_k]$ (= ρ_k / W_k) is the molar concentration of species k. The rate coefficients are typically given in Arrhenius form. However, due to a dearth of experimental data available in finite rate kinetics, the infinitely fast reaction mechanisms were adopted in order to simplify the combustion model.

Following an initial bursting charge explosion, a considerable amount of carbon dust, $C(s)$ and carbon monoxide, CO is generated with water vapor. When the $C(s)$ reacts with air at the blast front, it will generate CO, and then, if more oxygen is present, it will react to generate carbon dioxide, CO_2. Such mechanisms can be expressed by irreversible global reactions in Eq. (10).[7] When the aluminum particle is heated up above the ignition (or melting) temperature, the vaporized aluminum starts to participate in different combustion modes depending on the oxygen available. These modes are:

$$\begin{aligned} &C(s) + \frac{1}{2}O_2 \rightarrow CO \\ &CO + \frac{1}{2}O_2 \rightarrow CO_2 \\ &Al + \frac{3}{4}O_2 \rightarrow \frac{1}{2}Al_2O_3 - 810.3\ kJ \quad if\ T < 3500\ K \\ &Al + \frac{1}{2}O_2 \rightarrow AlO + 66.9\ kJ \quad if\ T \geq 3500\ K \\ &Al + \frac{3}{2}H_2O \rightarrow \frac{1}{2}Al_2O_3 + \frac{3}{2}H_2 + 475\ kJ \\ &Al + \frac{3}{2}CO_2 \rightarrow \frac{1}{2}Al_2O_3 + \frac{3}{2}CO + 413\ kJ \end{aligned} \tag{10}$$

where either the third or the fourth reaction equation above is an *aerobic* reaction[8] alternatively selected by the decomposition temperature of aluminum, and the fifth and sixth reaction equations are *anaerobic* reactions.[20]

To model high temperature and pressure explosive gas, we used the Noble-Abel EOS[7] considering the effects of finite volume molecules with a modified gas phase speed of sound.

2.2 Solid phase

For the dilute solid flow in a Lagrangian reference frame, the present model adopts the computational particle or discrete particle concept, each representing a finite number of child particles inside having the same diameter, velocity, and temperature.[10] The mass, momentum, and energy equation of the solid phase is given by enforcing the conservation law to an individual particle[21] During the momentum coupling process, the drag effects between particle and fluid are given as,

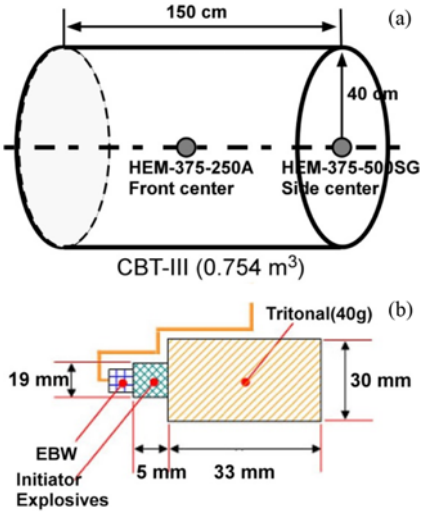

Fig. 1 Schematics of the experimental closed bomb test chamber and the structure of the initial TBX: a) closed bomb test chamber with volume of 0.754 m^3 with two pressure sensing positions at front and side center, and b) the TBX charge structure consists of 40 g of Tritonal and a blasting cap (initiator explosives, and an exploding bridge wire (EBW))

$$D_p(u_i) = 0.5\pi r_p^2 \rho C_D |u_i - u_{p,i}| \quad i = x,y,z \tag{11}$$

where C_D is the drag coefficient, typically determined by an empirical relation.[21]

For the model of the burning of aluminum particles, we employed an empirical quasi-steady law.[15]

$$\frac{dr_p}{dt} = -\frac{r_p}{t_b}(1 + 0.276\sqrt{Re_p}) \quad t_b = \frac{Kd_{p,0}^2}{\phi^{0.9}} \tag{12}$$

where t_b is the particle burning time, K the empirical evaporation rate constant, $d_{p,0}$ the initial particle diameter, and ϕ the volume fraction of oxidizing species in the surrounding gas.[15] Re_p is the particle Reynolds number evaluated with a relative velocity.

Since the ignition and burning rates are directly related to the different particle sizes,[21] we selected both a mono-dispersed and a poly-dispersed distribution (Rosin-Rammler), where the particles are distributed by referencing an average radius.

$$f(D) = 1 - \exp\left(-\frac{D^{3.5}}{\overline{D}}\right) \tag{13}$$

where $\overline{D}$ is the average diameter. A sampled particle distribution using Eq. (13) was confirmed with a manufactured one before it was used in simulation.

3. Experiment Validation

Experiments in present investigation were carried out using a closed bomb test (CBT) chamber for model validation of the TBX afterburning processes. Fig. 1 shows the schematics of the experimental chamber and an initial charge of TBX. The CBT chamber has a dimension of 40 cm in radius (r) and 150 cm in longitudinal length (x) so that the total volume of the chamber is 0.754 m^3. Two pressure gauges (Kulite; HEL-375-250A, and HEL-375-500A) having different sensing capacities were installed: one at the front enter of the cylinder (x = 750 cm, r = 40 cm) and the other at the side center of the cylinder base surface (x = 150 cm, r = 0 cm), respectively. The measured pressure data from the sensors were logged using the data acquisition system, DEWE-500, for analysis of the blast performance.

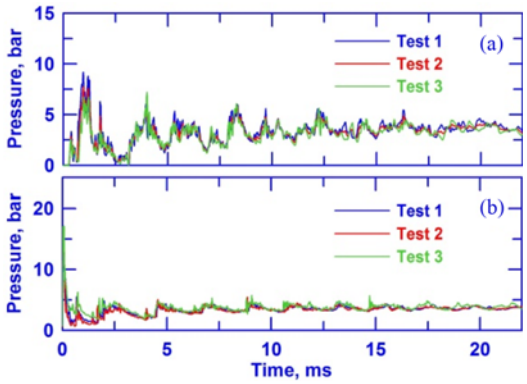

Fig. 2 Pressure histories as function of time after explosion collected from three different experiments: (a) side center (x = 150 cm, r = 0 cm), and (b) front center (x = 75 cm, r = 40 cm)

The cylindrical (30 mm in diameter and 33 mm in length) Tritonal TBX charge weighs 40 g and consists of well mixed TNT (80%) and aluminum particles (20%, with an average diameter of 10 μm). The main charge, combined with the blast cap (5 g booster explosives of TNT compounds) and the exploding bridge wire (EBW) shown in Fig. 1(b) was initially located at the CBT center (x = 75 cm, r = 0 cm) of the CBT chamber for each experiment. Several experiments were conducted to obtain reliable data sets, and three data sets were collected with less than 10% standard relative error (SRE) from the average at each time instant. The pressure histories after explosion are illustrated in Fig. 2 at the side (a) and front center (b) of the CBT chamber. The small deviations prove that the experimental data are reliable enough for model and simulation validation.

4. Results and Discussion

4.1 Initial conditions

For the cylindrical charge of TBX, an initiation of the detonation is triggered by igniting the initiator explosives using the EBW. With suitable conditions, and enough energy from the initiator, onset of detonation is developed in the TBX. In the present study, we assumed that the initial explosion (or detonation initiation process) was successful at the start of the calculation, similar to Ref. 7. Further discussion of the initiation process is beyond the scope of this paper.

Furthermore, by defining the blast volume (r_b = 2.75 cm) that contains the initial charge and its immediate surroundings, the initial explosion pressure and temperature are calculated by assuming a constant-volume well-stirred reactor. The initial mass fractions for the species are then determined by considering the stoichiometric global

Table 1 Initial condition

Species	Mole	Mass fraction
C(s)	0.49	0.18
O_2	0.00	0.00
CO	0.49	0.43
CO_2	0.00	0.00
Al	0.00	0.00
AlO	0.00	0.00
Al_2O_3	0.00	0.00
H_2O	0.35	0.20
H_2	0.00	0.00
N_2	0.22	0.19

T_{exp} = 2426 K, P_{exp} = 3132 bar

reaction with 32 g of TNT ($C_7H_5N_3O_6$),[4] assuming that the metal combustion starts far away from the origin of the charge because of the longer characteristic combustion time scale of an energetic metal particle.[9] Outside of the blast volume, the initial conditions are set with an ambient air condition. The mass fractions for the species involved and the explosion parameters are listed in Table 1. We also assumed that the initial particle velocities are zero for all classes of particles due to lack of experimental data. However, after a few simulation time steps, particles rapidly obtain their propagating momentum by interacting with the high speed blast waves. An unstructured 3D mesh of 13.5 million elements (0.3 million elements in a 2D axisymmetric mesh) is employed for the physical domain (one quadrant of half of the cylindrical volume), along with a maximum of 5000 discrete particles. The CE/SE Euler solver in LS-DYNA is used for the compressible gas simulation.

4.2 Blast performance

Prior to TBX simulation, the homogeneous calculation with only TNT explosive was conducted to better understand blast wave propagation and also to validate the developed code. Detailed geometrical setups and initial conditions can be found in Ref. 7. Although the results are not provided, the over pressure histories in time[7] was validated as a preliminary calculation.

Fig. 3 shows consecutive snapshots of the temperature distributions at different time instants showing the blast wave propagation procedures. After symmetric propagation and flame separation from a leading shock in Figs. 3(a) and (b), the shock wave hits the side walls and is reflected (Fig. 3(c)). Then, the flame starts to randomly mix as shown in Figs. 3(d)-(f). At later times, the flames become more chaotically mixed as seen in Figs. 3(g)-(i).

Fig. 4 shows the TBX validations with the pressure data sets for the side and front center position between the simulation results and averaged experimental data. Figs. 4(a) and (b) illustrate the pressure history at the side and front center, respectively, and Fig. 4(c) and (d) show the corresponding impulse, which is defined as pressure integrated over time.

When the blast waves arrives at the side center, the pressure immediately peaks to its maximum value, and the reflected wave from the cylinder wall results in the subsequent peaks as the process repeats, conjugates, and dissipates until the pressure converges to an elevated value, but still with considerably noisy patterns after 5 ms from the initial explosion. This phenomenon as shown in Fig. 4(b) is more

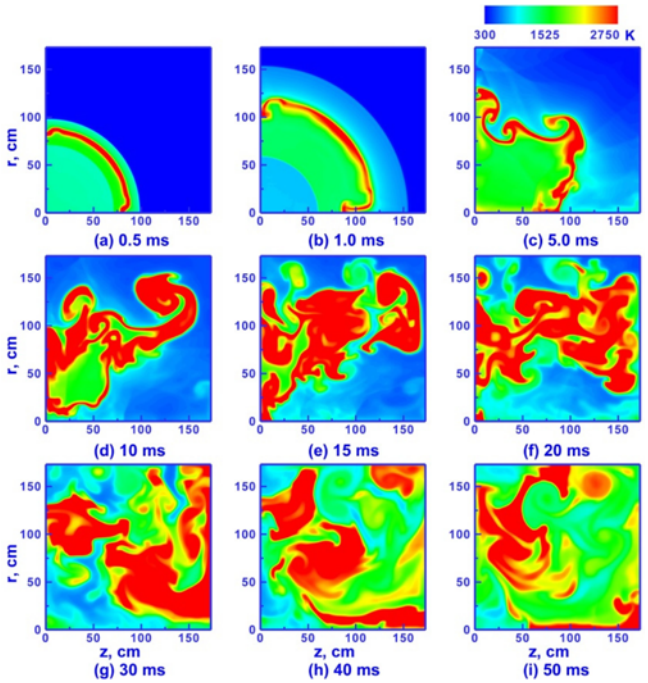

Fig. 3 Consecutive snapshots of the temperature distributions at different time for the blast propagation

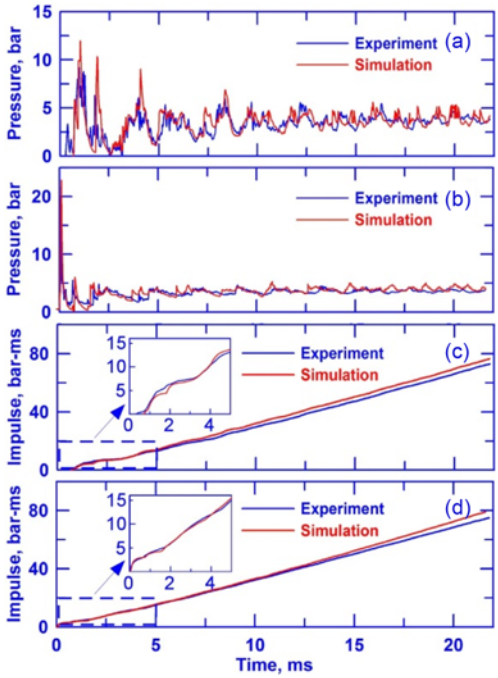

Fig. 4 Comparisons between measured data and simulation at the side and front center positions: (a) and (b) are the pressure histories, (c) and (d) are the impulses versus time

obvious at the front center location. Integrating the pressure with time, the corresponding impulses are smoother and gradually increasing, with very similar profiles both at the side and the front center locations. The only distinguishable patterns are detected for the earlier time period with more dynamic impulse acting on the side center, as shown

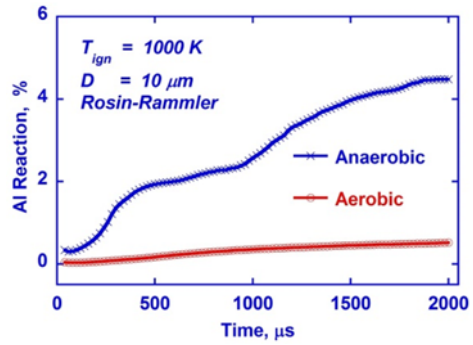

Fig. 5 Consumed aluminum gases by aerobic and anaerobic reaction

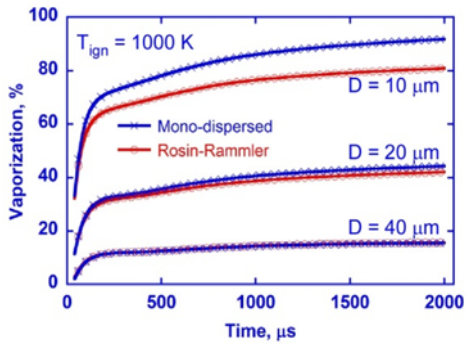

Fig. 6 Aluminum vaporization rate according to particle distribution and different particle diameters

in the magnified boxes in Fig. 4(c) and (d).

It is clear that the simulation results are in excellent agreement with the experimental data over the time ranges. At earlier time, the peak pressures slightly overshoot the measured data. In general, when the metal particles contribute to the afterburning in TBX, the peak pressure becomes lower but the impulse tends to be higher as the chamber pressure lasts longer than that of normal high explosives. While it could be argued that the metal combustion is less active or under-predicted in the simulation, the impulse profiles showed particularly good agreement, which suggests that the deviation may come from a different source rather than particle combustion. Indeed, since our simulation was based on an Euler solver, there may be possible viscous effects on the propagating blast wave in the surrounding air.

As the metal particles propagate into the surrounding air and interact with high temperature gaseous detonation products, some of the particles meet the ignition condition by generating vaporized aluminum gas and reacting according to the burning law and the reaction mechanisms whether with oxygen or detonation products. The former aerobic reaction with oxygen happens only at the blast front, and the latter anaerobic reaction without oxygen takes place behind the blast gas, which mainly contributes to the afterburning performance. Comparisons between them are illustrated in Fig. 5 for the case with a Rosin-Rammler particle distribution with a mean diameter of 10 μm, and ignition temperature at 1000 K. Obviously, much of the vapor reacted anaerobically, whereas only a small amount of the aluminum gas is consumed by the aerobic reaction mode in the combustion. This is very plausible since the blast front sweeps with supersonic speeds and reacts mostly two-dimensionally, while the bulk afterburning has more time and space to continue. However, the total amount of aluminum vapor reacted is quite small in both cases. In general, the most active aluminum reaction in the confined chamber happens before reflection (the distance from the initial charge to the wall). But it should continue to react if the temperature is high enough, coupled with sufficient reactants.

4.3 Particle dynamics

Fig. 6 illustrates the effects of particle dynamics on aluminum vaporization by varying the initial conditions such as mono-dispersed and Rosin-Rammler distributions, and different particle mean diameters, 10 μm, 20 μm, and 40 μm. The mono-dispersed distributions show a higher rate of vaporization in all cases. The deviations from the vaporization curves between the distributions are reduced with increasing

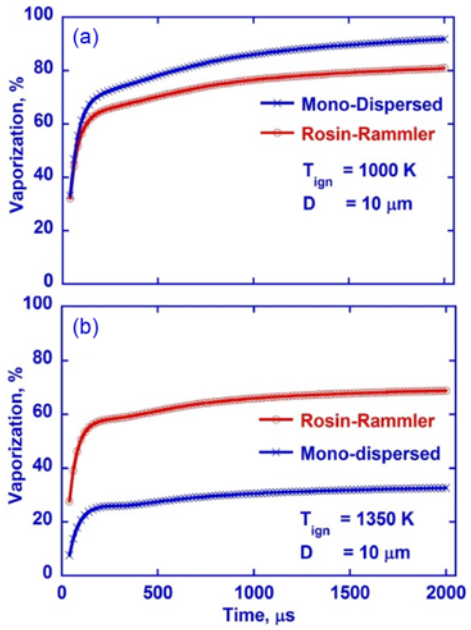

Fig. 7 Comparisons of aluminum vaporizations according to ignition temperatures with different particle distributions: (a) T_{ign} = 1000 K and (b) T_{ign} = 1350 with the particle diameter of 10 μm

diameter and eventually, there is little difference in the 40 μm cases, in which the size distribution is no longer important in confined explosions. It is also obvious that the vaporization rates decrease almost linearly with increasing diameter. At 10 μm, the particle vaporization is about 80% of the initial aluminum particle mass. With doubled diameter, it is approximately reduced by factor of two. At 40 μm, it is cut down another half, much less than 20%. From these observations, the maximum contribution of metal combustion to the afterburning performance occurred at small particle diameter. But there might be a critical diameter to optimize the afterburning performance. Therefore, the proper selection of the particle diameter is of paramount importance in the manufacturing process of TBX.

Fig. 7 compares the vaporization rate in time between two different ignition temperatures, (a) T_{ign} = 1000 K and (b) T_{ign} = 1350 K for different initial distributions. Since the melting point of aluminum is about 933 K, the ignition temperature of 1000K looks more reasonable.

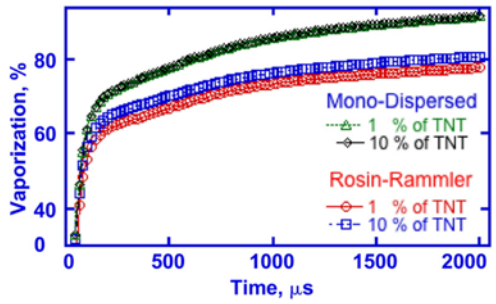

Fig. 8 Effect of aluminum particle percentages on the vaporization rate with 1% and 10% of TNT mass on different particle distributions: mono-dispersed and Rosin-Rammler at the ignition temperature of 1000 K and the mean diameter of 10 μm

On the other hand, Benkiewicz and Hayashi[8] employed 1350 K. The mono-dispersed distribution shows more sensitive variation with changing ignition temperature. By contrast, the Rosin-Rammler distribution shows less sensitivity with a considerable amount of vaporization (@60%), guaranteeing good afterburning performance. Obviously, the poly-dispersed distribution is a more physical and realistic choice for the afterburning of TBX combustion.

Fig. 8 shows the effect of aluminum particle percentages for the vaporization rate on the different particle distributions, with 1% and 10% of TNT mass: mono-dispersed and Rosin-Rammler. Here we used the mean diameter of 10 μm and the ignition temperature set to 1000 K. In the mono-dispersed case, although the amount of aluminum particle is changed by a factor of 10, the vaporization rate curve is not distinctive. By contrast, considerable changes of the vaporization rate curves are detected for the Rosin-Rammler distribution. Nevertheless, it is interesting to see that the high percentage of vaporization, more than 60% happens for the earlier stage of combustion, and the gradually increasing curves of the vaporization rate are observed regardless of the particle percentages for the remaining time.

5. Conclusion

In summary, the present investigation has demonstrated an accurate and concrete model developed for the afterburning process of TBX combustion in conjunction with experimental validation in a confined chamber. Based on the results for the afterburning performance, our multiphase solver showed moderately good agreement with experimental data, and furthermore, the selection of the aluminum burning rate law proved to be reasonable. From the particle dynamics results, it is demonstrated that careful choice of the average particle size is critical to maximize blast performance and in particular, a poly-dispersed particle distribution is the more physical and promising choice to guarantee better afterburning performance. Therefore, the simulation for the afterburning of TBX, validated by the experimental data, clearly revealed the importance of variable selections such as particle burning model, the particle mean size, and its distribution, for the optimum blast performance, which should find broader applications in related industries.

ACKNOWLEDGEMENT

The authors acknowledge Won-Ho Cho, Hee-Sung Yang, and Sang Young Lee from SAMYANG Chemical Co., Ltd., Korea for providing the experimental data used in the current study, as well as helpful discussions.

REFERENCES

1. Kim, K., Wilson, W., Colon, J., Kreitinger, T., Needham, C., et al., "Non-Ideal Explosive Performance in a Building Structure," in: Design against Blast: Load Definition & Structural Response, Syngellakis, S., (Ed.), WIT Press, pp. 87-95, 2013.
2. Massoni, J., Saurel, R., Lefrancois, A., and Baudin, G., "Modeling Spherical Explosions with Aluminized Energetic Materials," Shock Waves, Vol. 16, No. 1, pp. 75-92, 2006.
3. Price, E. W., Sigman, R. K., Sambamurthi, J. K., and Park, C. J., "Behavior of Aluminum in Solid Propellant Combustion," Georgia Institute of Technology, AD A118128, 1982.
4. Kim, C.-K. and Hwang, J. S., "Numerical Modeling for the Performance Prediction of Thermobaric Explosive," Proc. of 1st KISEM, 2009.
5. Kim, C.-K., Hwang, J.-S., and Im, K.-S., "Numerical Simulation of Afterburning of Thermobaricexplosive Products in Air," Proc. of 23rd International Symposium on Ballistics, Tarragona, pp. 201-208, 2007.
6. Kim, C.-K., Moon, J. G., Lai, M.-C., and IM, K.-S., "Afterburning of TNT Explosive Products in Air with Aluminum Particles," Proc. of 46th AIAA Aerospace Sciences Meeting and Exhibit, AIAA 2008-1029, 2008.
7. Schwer, D. and Kailasante, K., "Blast Mitigation by Water Mist (1) Simulation of Confined Blast Waves," Naval Research Laboratory, Report No. NRL/MR/6410-02-8636, 2002.
8. Benkiewicz, K. and Hayashi, K., "Two-dimensional Numerical Simulations of Multi-Headed Detonations in Oxygen-Aluminum Mixtures Using an Adaptive Mesh Refinement," Shock Waves, Vol. 12, No. 5, pp. 385-402, 2003.
9. Zhang, F., Frost, D. L., Thibault, P. A., and Murray, S. B., "Explosive Dispersal of Solid Particles," Shock Waves, Vol. 10, No. 6, pp. 431-443, 2001.
10. Dukowicz, J. K., "A Particle-Fluid Numerical Model for Liquid Sprays," Journal of Computational Physics, Vol. 35, No. 2, pp. 229-253, 1980.
11. Brzustowski, T. and Glassman, I., "Vapor-Phase Diffusion Flames in the Combustion of Magnesium and Aluminum. I-Analytical Developments," Proc. of Heterogeneous Combustion Conference, Paper No. 489, 1963.
12. Law, C. K., "A Simplified Theoretical Model for the Vapor-Phase

Combustion of Metal Particles," Combustion Science and Technology, Vol. 7, No. 5, pp. 197-212, 1973.

13. Glassman, I., "Metal Combustion Processes," Princeton University, ARS Preprint No. 938-59, 1959.
14. Needham, C., Crepeau, J., and Caipen, T., "A Computational Aluminum Particulate Burn Model," MABS 17, Session VIII, P02, 2002.
15. Khasainov, B., and Veyssiere, B., "Steady, Plane, Double-Front Detonations in Gaseous Detonable Mixtures Containing a Suspension of Aluminum Particles," Progress in Astronautics and Aeronautics, Vol. 114, pp. 284-299, 1988.
16. Zhang, F., Gerrard, K., and Ripley, R. C., "Reaction Mechanism of Aluminum-Particle-Air Detonation," Journal of Propulsion and Power, Vol. 25, No. 4, pp. 845-858, 2009.
17. Zhang, Z.-C., Yu, S. J., and Chang, S.-C., "A Space-Time Conservation Element and Solution Element Method for Solving the Two- and Three-Dimensional Unsteady Euler Equations Using Quadrilateral and Hexahedral Meshes," Journal of Computational Physics, Vol. 175, No. 1, pp. 168-199, 2002.
18. Crowe, C. T., Schwarzkopf, J. D., Sommerfeld, M., and Tsuji, Y., "Multiphase Flows with Droplets and Particles," CRC Press, 2011.
19. Gordon, S. and McBride, B. J., "Computer Program for Calculation of Complex Chemical Equilibrium Compositions, Rocket Performance, Incident and Reflected Shocks, and Chapman-Jouguet Detonations," NASA, No. SP-273, 1976.
20. Okhitin, V. N., Selivanov, V. V., and Zibarov, A. V., "Combustion of Energetic Materials," Begell House, New York, pp. 1072-1089, 2002.
21. Faeth, G., "Current Status of Droplet and Liquid Combustion," Progress in Energy and Combustion Science, Vol. 3, No. 4, pp. 191-224, 1977.